APPLIED OPTICS

# Single-crystalline germanium nanomembrane photodetectors on foreign nanocavities

Zhenyang Xia,[1]* Haomin Song,[2]* Munho Kim,[1]* Ming Zhou,[1] Tzu-Hsuan Chang,[1] Dong Liu,[1] Xin Yin,[3] Kanglin Xiong,[1] Hongyi Mi,[1] Xudong Wang,[3] Fengnian Xia,[4] Zongfu Yu,[1†] Zhenqiang (Jack) Ma,[1†] Qiaoqiang Gan[2†]



**Miniaturization of optoelectronic devices offers tremendous performance gain. As the volume of photoactive material decreases, optoelectronic performance improves, including the operation speed, the signal-to-noise ratio, and the internal quantum efficiency. Over the past decades, researchers have managed to reduce the volume of photoactive materials in solar cells and photodetectors by orders of magnitude. However, two issues arise when one continues to thin down the photoactive layers to the nanometer scale (for example, <50 nm). First, light-matter interaction becomes weak, resulting in incomplete photon absorption and low quantum efficiency. Second, it is difficult to obtain ultrathin materials with single-crystalline quality. We introduce a method to overcome these two challenges simultaneously. It uses conventional bulk semiconductor wafers, such as Si, Ge, and GaAs, to realize single-crystalline films on foreign substrates that are designed for enhanced light-matter interaction. We use a high-yield and high-throughput method to demonstrate nanometer-thin photodetectors with significantly enhanced light absorption based on nanocavity interference mechanism. These single-crystalline nanomembrane photodetectors also exhibit unique optoelectronic properties, such as the strong field effect and spectral selectivity.**

## INTRODUCTION

Recently, ultrathin semiconductors [for example, silicon (Si)/germanium (Ge) nanomembranes (*1*, *2*) and two-dimensional (2D) materials (*3*–*5*)] have emerged as attractive building blocks for miniaturized optical/optoelectronic devices. To enhance the light-matter interaction, thin-film interference in lossy, ultrathin semiconductor layers received extensive research efforts (*6*) due to their potential applications for integrated optical filters (*7*, *8*), high-efficiency ultrathin-film energy-harvesting devices (*9*), energy conversion materials/structures (*10*, *11*), and dynamic wave–shaping metasurfaces (*12*). For instance, Ge thin films (1 to 20 nm) were coated on flat metal films to exploit strong interference effects and achieve high absorption (that is, 65 to 95%) at resonant wavelengths in the visible–to–near-infrared spectral region (*13*). However, all these works are based on amorphous semiconductors. Consequently, their optoelectronic device performance (*14*) is far inferior to those crystalline material–based counterparts. Although single-crystalline films can be obtained through rapid melt growth (RMG) (*15*, *16*), wafer bonding (*17*), and/or epitaxial growth (*18*, *19*), each of these methods has its limitations. For example, the RMG method will introduce high-temperature process flow (>900°C) to recrystallize the Ge material. The wafer bonding method will require the substrate removal after the process, and the epitaxial growth needs very thick buffer layers. Fabrication of crystalline thin films on foreign substrates turns out to be critically important for ultrathin optoelectronics. The recently emerging membrane transfer technology provides a promising way to enable the combination of crystalline thin films with foreign substrates (*20*, *21*). In particular, the foreign substrate can be designed with effective photon-management functionalities to greatly enhance the weak light absorption in ultrathin materials. Here, we demonstrate a new method to realize high-performance ultrathin optoelectronic devices based on nanocavity-enhanced mechanisms. Using single-crystalline semiconductor membranes on functionalized nanocavity substrates, we achieve strong light-matter interaction within nanometer-thick Ge films. Although we use Ge as an example to demonstrate a high-performance photodetector, our method can be applied to other semiconductors, including two-dimensional (2D) materials (*22*, *23*), to enable the development of improved ultrathin optical/optoelectronic devices.

## RESULTS

### Ultrathin crystalline Ge on foreign substrates

Here, we first used the membrane transfer method (*20*, *21*) to realize the integration of crystalline semiconductor films with a foreign substrate, as shown in Fig. 1A. We started from a Ge-on-insulator (GeOI) wafer as the source wafer (Fig. 1A, i, and figs. S1 to S3; see Materials and Methods). The thicknesses of the top Ge layer and the insulator layer of $SiO_2$ are 100 nm and 1 μm, respectively. We then released the top Ge membrane using hydrofluoric acid (Fig. 1A, ii) and transferred it onto a foreign substrate using polydimethylsiloxane (Fig. 1A, iii). Finally, we used low-power dry etching to thin down the membrane to the desired thickness (Fig. 1A, iv). Figure 1B shows the optical microscopy images of transferred Ge membrane samples. The substrate was designed to enhance the light absorption in Ge membranes. It consists of three layers: a top $Al_2O_3$ layer, a middle silver (Ag) layer, and a Si substrate. The top Ge film thickness, measured by atomic force microscopy (AFM) (fig. S4), ranges from 10 to 60 nm. These films exhibit different colors under white light illumination because of the optical interference (Fig. 1B and figs. S5 and S6).

To reveal the crystal quality of the Ge membrane, we performed high-resolution x-ray diffraction (HR-XRD) characterization. Figure 1C

[1]Department of Electrical and Computer Engineering, University of Wisconsin-Madison, WI 53706, USA. [2]Department of Electrical Engineering, University at Buffalo, State University of New York, Buffalo, NY 14260, USA. [3]Department of Materials Science and Engineering, University of Wisconsin-Madison, Madison, WI 53706, USA. [4]Department of Electrical Engineering, Yale University, New Haven, CT 06511, USA.
*These authors contributed equally to this work.
†Corresponding author. zyu54@wisc.edu (Z.Y.); mazq@engr.wisc.edu (Z.M.); qqgan@buffalo.edu (Q.G.)

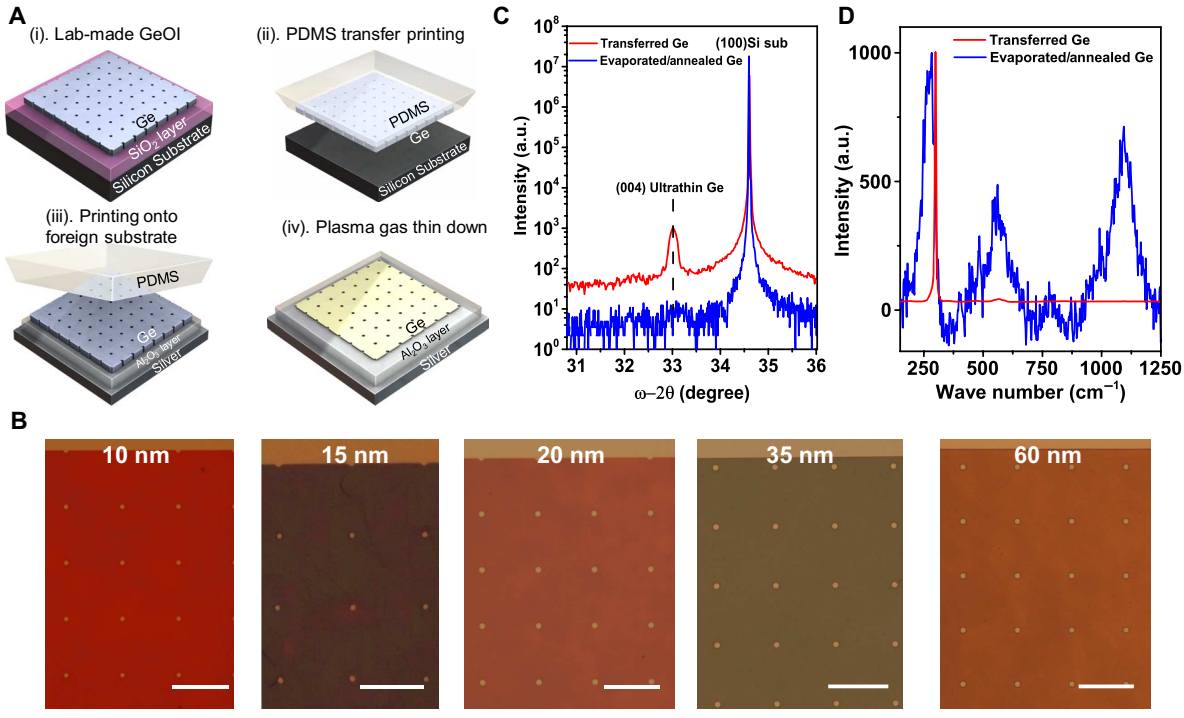


**Fig. 1. Fabrication and characterization of ultrathin Ge nanomembranes on foreign substrates.** (**A**) Schematic of the fabrication process flow of the Ge nanomembranes on foreign substrates. The laboratory-made GeOI was used as the source wafer, and the membrane transfer–printing method (figs. S5 and S6) was then used to transfer the Ge membrane onto a foreign substrate. Subsequent thin-down process was adopted to obtain the desired Ge thickness (10 to 60 nm). (**B**) Optical microscopy image of ultrathin Ge (10 to 60 nm), which is transfer-printed on $Al_2O_3$/Ag/Si substrates. Scale bars, 75 μm for all five subfigures. (**C**) Triple-axis HR-XRD scans of our transferred crystalline ultrathin Ge (red) and evaporated amorphous Ge (blue) films. The thicknesses are both 20 nm. (**D**) Raman scattering results of the two samples in (C). The Raman signal of the transferred Ge membrane shows the typical single peak (300.9 $cm^{-1}$) of single-crystalline Ge materials.

shows the (004) ω-2θ triple-axis scans. A clear peak at 33.1° (red line) confirms the single crystallinity of transferred Ge membranes (*24*). In comparison, we also examined an evaporated and annealed Ge film with the same thickness. Here, the evaporated amorphous Ge film was annealed at 500°C to improve the crystallinity (*25*). This type of polycrystalline Ge film was typically used to fabricate Ge photodetectors on foreign substrates using low-temperature processes (*26*). However, no peak was observed at 33.1° for the blue line in Fig. 1C, which indicated the lack of single crystallinity. This comparison reveals the advantage of our membrane transfer method in the quality of Ge films, which is important for the performance of photodetectors. Another peak in Fig. 1C at the angle of 34.6° comes from the (100) Si substrate, which is observed in both samples. Figure 1D shows the Raman spectroscopy of these two samples. One can see a single peak at the wave number of 300.9 $cm^{-1}$ for the transferred Ge membrane, which is another signature of the single-crystalline Ge film (*27*). In contrast, multiple peaks were observed in the evaporated and annealed Ge film. These peaks are attributed to the Ge-$H_x$ and second order of Ge-Ge bonds formed in the annealing process (*28*). Both the XRD and Raman results show excellent crystalline properties of the transferred Ge films. Next, we discuss the design of the foreign substrate to enhance the light-matter interaction within this crystalline thin film.

## Foreign substrate with effective photon management

Predesigned foreign substrates allow us to use a functionalized nanocavity structure to greatly improve the light absorption in nanometer-thin Ge films. The absorption depth of Ge varies from approximately 120 nm (at the wavelength of 700 nm) to 390 nm (at the wavelength of 900 nm), much thicker than our thin films. In this case, the absorption in a 20-nm-thick region is less than 16% in this wavelength range. To overcome this limitation of weak absorption, we use a layered substrate that consists of a 220-nm-thick lossless dielectric spacer and a reflective Ag mirror to form a functionalized nanocavity structure (Fig. 2A). As shown by the solid line in Fig. 2B, the simulated absorption in a 20-nm-thick Ge membrane on a 220-nm-thick $Al_2O_3$/Ag cavity reaches 81% around the resonant wavelength of 733 nm. The spatial distribution of light absorption, obtained in a simulation based on the finite element method, shows enhanced absorption in the ultrathin layer of Ge (Fig. 2C). In contrast, the absorption in ultrathin crystalline Ge films without photon management is weak. For example, ultrathin crystalline Ge films can also be fabricated using epitaxial growth [for example, see the study of Wang and Lee (*29*), as illustrated in Fig. 2D]. However, the substrate should be a $Si_{0.75}Ge_{0.25}$ buffer layer [its optical constants (*n* and *k*) are obtained from the semiconductor archive website (*30*)] to fulfill the lattice matching condition. Under this situation, the same Ge film only absorbs less than 10% of the incident light at 733 nm, as shown in Fig. 2E. The spatial distribution of light absorption in this system is shown in Fig. 2F, with the same color map in Fig. 2D, showing obviously weaker absorption within the 20-nm-thick Ge film. Therefore, the foreign nanocavity substrate can significantly enhance the optical absorption within the ultrathin crystalline film, which is highly desirable for optoelectronic devices.

## Nanocavity-enhanced photodetector

The schematic of a nanocavity-enhanced photodetector device and its optical microscopy image are shown in Fig. 3 (A and B, respectively). We first fabricated this device and measured its performance under

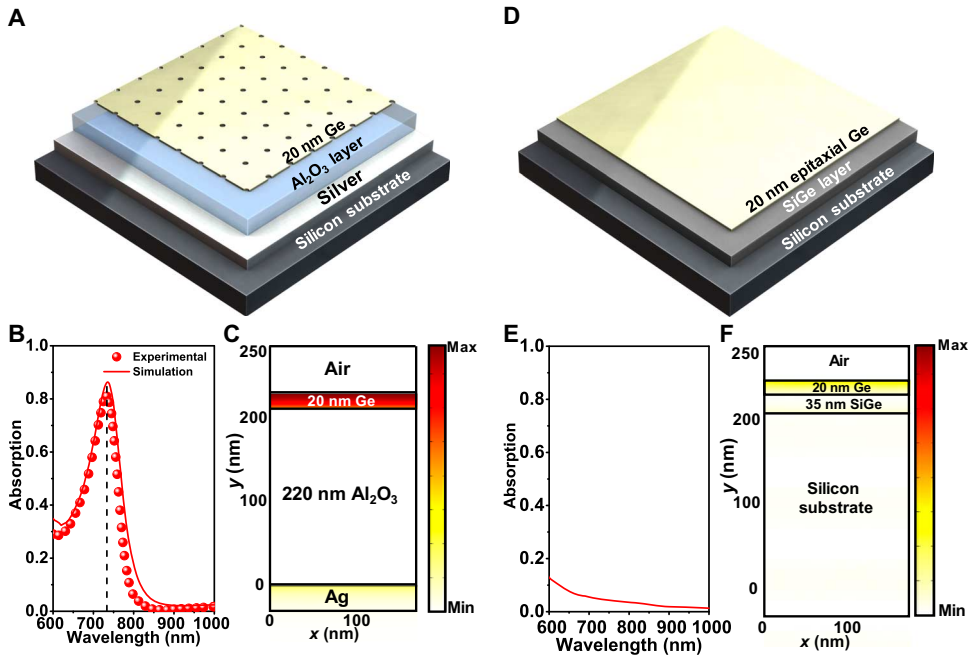


**Fig. 2. Absorption results of ultrathin Ge nanomembrane on foreign substrate and its comparison with a traditional structure.** (**A**) Schematic of ultrathin Ge (20 nm) nanomembrane on the foreign substrate. (**B** and **C**) Absorption spectra (B) and the spatial distribution of the absorption (C) for the structure shown in (A). (**D**) Schematic of a traditional epitaxial Ge on $Si_{0.75}Ge_{0.25}$ buffer layer/Si substrate. (**E** and **F**) Absorption spectrum (E) and the spatial distribution of the absorption (F) for the structure shown in (D). The color bars in (C) and (F) use the same scale for direct comparison.

dark and illuminated conditions. Here, we placed a 17-nm-thick p-type (gallium-doped) Ge nanomembrane on a 220-nm-thick $Al_2O_3$/Ag cavity and obtained an absorption peak at 733 nm (dotted line in Fig. 2B), agreeing well with the theoretical prediction (solid line in Fig. 2B). The slight difference in Ge film thickness should be attributed to the optical constant difference of this p-type Ge film. In particular, the bottom Ag film serves a dual role of mirror and gate electrode for this nanomembrane-based field-effect transistor device. By using nickel/gold (Ni/Au) as the contact electrode, we realized an ohmic-like contact for the photoconductor, as shown by the current-voltage (*I-V*) sweep results in Fig. 3C. We repeated the *I-V* sweep under different illumination intensities by tuning the monochromatic 733-nm light source from 42 nW to 2.45 μW. All the *I-V* curves under the dark and illumination conditions show nonlinear behavior, which is caused by nonideal ohmic contacts (a potential barrier exists) of metal with the ultrathin Ge. As $V_{DS}$ increases, more and more voltage will drop at the metal/Ge interface, which makes the increase of the current nonlinear. The photocurrent ($|\Delta I_{DS}|$) at the bias of 1 V can be calculated by the equation $|\Delta I_{DS}| = |I_{DS} - I_{dark}|$, where $I_{DS}$ is the drain-source current under illumination and $I_{dark}$ is the dark current. We then plotted the photocurrent, $|\Delta I_{DS}|$, as the function of the incident power, $P_{inc}$, illuminated on the ultrathin Ge layer (25 μm × 50 μm), as shown in the inset of Fig. 3C. From the linear fitting of the photocurrent with the illuminated power, we can extract the photoresponsivity ($R$) of this device to be 0.17 A/W (that is, $R = |\Delta I_{DS}|/P_{inc}$).

## Stable and improved normalized photocurrent–to–dark current ratio

One important figure of merit for metal-semiconductor-metal (MSM) photodetectors is the normalized photocurrent–to–dark current ratio [NPDR = $(|\Delta I_{DS}|/I_{dark})/P_{inc}$] (*31*). A larger value of this parameter indicates the better suppression of dark current without sacrificing the photoresponsivity. Considering the previously reported MSM photodetector based on Ge wafers (*32*), the highest reported NPDR, to our knowledge, was 3158 $mW^{-1}$. In contrast, under the bias of 1 V, the NPDR of our device is in the range of $10^4$ $mW^{-1}$ (red dots in Fig. 3D), which is more than one order of magnitude higher than the previous work. Here, we first investigated the stability of the NPDR by increasing the incident power, $P_{inc}$. One can see that the NPDR of our ultrathin Ge sample is relatively stable in the power range from 42 nW to 2.45 μW (Fig. 3D). For comparison, we also plotted the NPDR of a previously reported 2D material device based on $MoS_2$ (blue dots) (*33*). This device has an NPDR with a significant change, from a value of $6.37 \times 10^4$ $mW^{-1}$ at the low incidence power to $2.39 \times 10^3$ $mW^{-1}$ (that is, one order of magnitude lower) when the incidence power reaches the microwatts level (*33*). This drop was attributed to the saturation of the trap states with increased light intensity. Therefore, the stable NPDR of our nanocavity sample in the investigated incidence power range demonstrates the high quality of the single-crystalline Ge nanomembranes.

In addition to the stability of NPDR, the enhanced NPDR, compared with one previously reported (*32*), can be attributed to two mechanisms. The first one is the suppression of the dark current, $I_{dark}$, introduced by the ultrathin Ge film. To verify the suppression, we fabricated the photoconductors with various Ge thicknesses and measured their dark currents (see fig. S7). As shown in Fig. 3E, the dark current at the bias of 1 V decreases from the milliampere to nanoampere level as the Ge thickness reduces from 350 to 20 nm. The marked drop of the dark current when the thickness of Ge films decreases down to ~20 nm is caused by the effect of depleted charges in ultrathin films (*34*). In general, ultrathin Ge nanomembranes intrinsically bring about low absorption, which limits the photocurrent, $|\Delta I_{DS}|$, and thus results in a relatively small NPDR. By introducing the foreign nanocavity, however, the absorption will be significantly enhanced, corresponding to enhanced

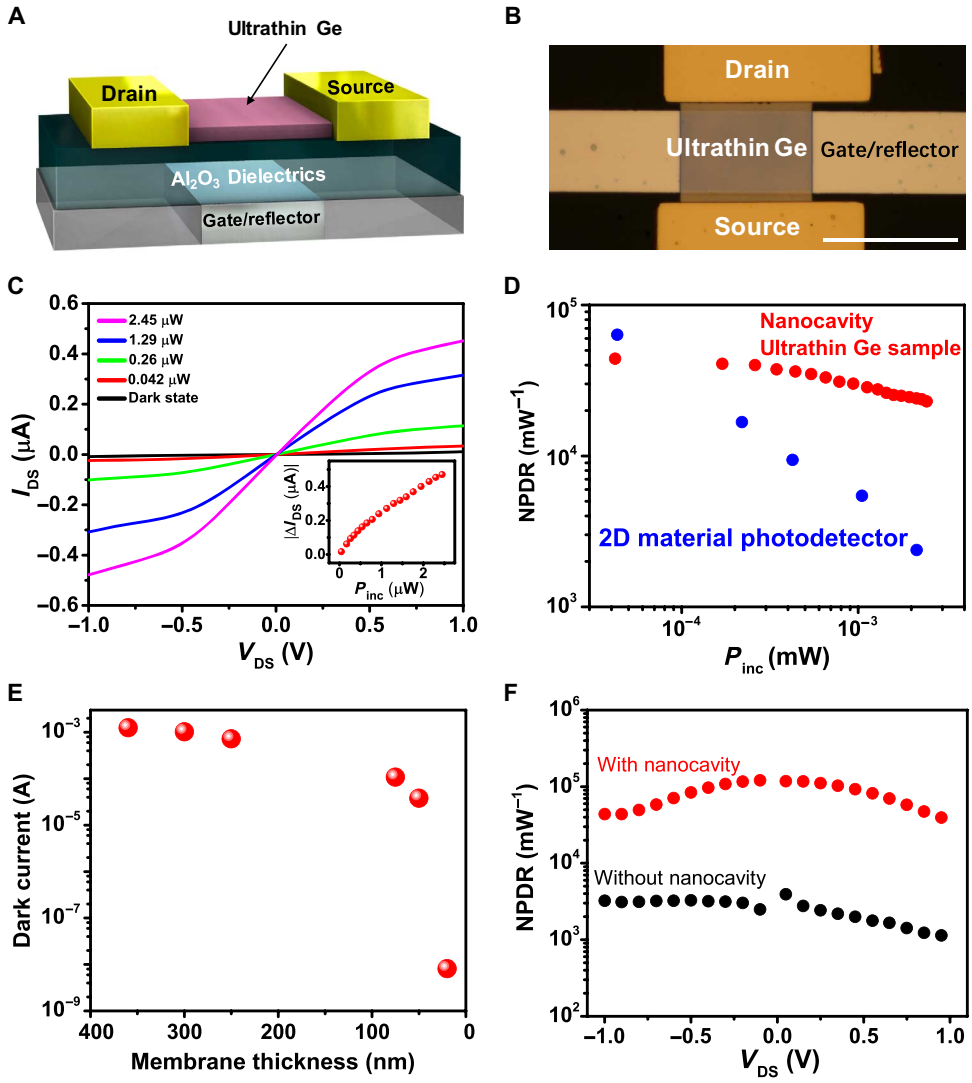


**Fig. 3. *I-V* measurements of ultrathin Ge photodetector under both dark and illuminated conditions.** (**A**) Schematic of an ultrathin Ge photodetector on a nanocavity. (**B**) Optical microscopy image of ultrathin Ge photodetector. Scale bar, 50 μm. (**C**) *I-V* curves of the p-type Ge photoconductor under dark (black curve) and illuminated (colored curves) conditions. Inset: The photocurrent shows a linear relationship with the illuminated power. (**D**) Calculated normalized photocurrent–to–dark current ratio (NPDR) with the illuminated power and its comparison with a $MoS_2$ photodetector. (**E**) Dark current of Ge membranes with different thicknesses (that is, 360, 300, 250, 75, 50, and 20 nm) under the bias of 1 V. (**F**) NPDR comparison between the Ge photodetectors with and without nanocavity structure (GeOI-based).

photocurrent, which is the second reason for the improved NPDR. To better reveal the dependence of NPDR on absorption, we fabricated another photodetector constituted by a GeOI structure. The thickness of the $SiO_2$ in the GeOI sample is 1 μm (fig. S8). Because the thickness of the Ge film is similar to that in the nanocavity sample (that is, 20 nm), the dark currents of the two samples were suppressed to a similar level. Figure 3F shows the comparison of NPDR between these two photodetectors. Under the same bias, one can see that the nanocavity sample delivers one order of magnitude higher NPDR (that is, ~$4 \times 10^4$ $mW^{-1}$) than that of the GeOI sample (~$3 \times 10^3$ $mW^{-1}$). With respect to absorption, the absorption in the Ge layer of the nanocavity sample is 81% (see Fig. 2B), which is also one order of magnitude larger than that of the GeOI sample (6.1%, based on our simulation), demonstrating the contribution of the enhanced absorption to NPDR. Furthermore, the gate-controlled performance of the phototransistors also takes advantage of the high absorption, as will be analyzed in the next section.

## Device physics

### *General electronic properties of the single-crystalline nanomembrane transistor*

To further interpret the electronic properties of the single-crystalline Ge nanomembrane transistor, we then characterized the dark drain-source current, $|I_{DS}|$, of the device with the 17-nm-thick Ge film (discussed in Fig. 3) as the function of the gate voltage, $V_{GS}$, under $V_{DS}$ of −1 V. As shown by the dashed blue curve plotted in the log scale in Fig. 4A, the ultrathin transistor shows ambipolar behavior. By extrapolating the linear portion of the $I_{DS}$-$V_{GS}$ curve in the linear scale (red solid curve), one can extract the threshold voltage of the transistor, $V_{TH}$. Furthermore, one can estimate the hole field-effect mobility, $\mu_p$, using the equation $\mu_p = (L/W)C_{ox}^{-1}V_{DS}^{-1}(\partial I_{DS}/\partial V_{DS})$, where $L$ and $W$ are the Ge nanomembrane channel length and width (that is, 25 and 50 μm), respectively, and $C_{ox}$ is the gate capacitance per unit area of the Ge/$Al_2O_3$/Ag system (that is, $3.647 \times 10^{-8}$ $F/cm^2$), determined by the expression

$C_{ox} = \varepsilon_{ox}/t_{ox} = \varepsilon_o\varepsilon_{Al2O3}/t_{Al2O3}$. Here, $\varepsilon_o$ is the vacuum absolute dielectric constant (that is, $8.85 \times 10^{-12}$ F/m), $\varepsilon_{Al2O3}$ is the relative $Al_2O_3$ dielectric constant [that is, 8.1 for the evaporated $Al_2O_3$ layer (*35*)], and $t_{Al2O3}$ is the thickness of the $Al_2O_3$ layer (that is, 220 nm). As a result, the maximum $\mu_p$ of this 17-nm-thick Ge membrane transistor can be estimated to be ~148.1 $cm^2 V^{-1} S^{-1}$ in the linear portion when $V_{GS}$ varies from −5 to −7.5 V (as indicated by the black line in Fig. 4A). This value is among the best reported results (*36*–*41*) due to the single-crystalline material quality. Intriguingly, this nanocavity-manipulated device has unique properties on its gate-controlled responses, as will be discussed next.

### *Gate-controlled photocurrent response*

To reveal the gate-controlled optical response of this device, we then swept the $V_{DS}$ under different $V_{GS}$ in a steady optical incidence condition of 140.8 mW/$cm^2$. As shown in Fig. 4B, the photocurrent $|\Delta I_{DS}|$ increases as $V_{GS}$ decreases from −2 to −6 V. In particular, when $V_{DS}$ = −1.5 V and $V_{GS}$ = −6 V, the photoresponsivity is 4.7 A/W, which is 27.6 times larger than the responsivity of 0.17 A/W under zero gate voltage. This enhancement can be attributed to the photogating effect, which plays a dominant role in many nanostructured devices, especially in nanowires (*42*), quantum dots (*43*), and 2D material–based photodetectors (*44*). However, in most of the aforementioned devices, the photogating effect relies on trap states in nanostructured materials, acting as localized states in the photodetecting channel. The trap state–mediated photogating effect limits the reproducibility of the photodetector performance because the number of trap states cannot be controlled precisely in the fabrication process. Moreover, the saturation of the trap states under strong incident power usually resulted in decreased gain (*45*).

In contrast, the photogating effect in our developed cavity-manipulated ultrathin nanomembrane phototransistor is majorly due to the high optical absorption and corresponding photogenerated carriers confined within the ultrathin Ge films. The high absorption at the desired wavelength can be precisely controlled by tuning the thickness of either the Ge or $Al_2O_3$ layers. The absorbed photons generate carriers confined in the Ge channel, therefore resulting in the improved photoconductivity. To reveal the photogating effect quantitatively [that is, $|\Delta I_{DS}| = |G_m|\Delta V_{TH}$ (*46*), where $\Delta V_{TH}$ is the photon-induced change of the threshold voltage], we then analyze the relation of the photocurrent, $|\Delta I_{DS}|$, with the device transconductance, $|G_m|$ ($|G_m| = |\partial I_{DS}/\partial V_{GS}|$), which can be extracted from Fig. 4A, as shown in the lower panel of Fig. 4C. Here, we swept the gate voltage $V_{GS}$ under $V_{DS}$ at −1 V and extracted $|\Delta I_{DS}|$ resulted from $\Delta V_{TH}$ under different optical illumination conditions, as shown by the curves in the upper panel of Fig. 4C (fig. S9). One can see that these $|\Delta I_{DS}|$-$V_{GS}$ curves are consistent with the $|G_m|$-$V_{GS}$ curve, confirming that the gate-controlled photocurrent results from the photogating effect (*46*).

In addition, the photogating effect expression (that is, $|\Delta I_{DS}| = |G_m|\Delta V_{TH}$) shows that with a given $V_{GS}$, a bigger change of threshold voltage, $\Delta V_{TH}$, leads to a larger photocurrent, $|\Delta I_{DS}|$. To compare our device with a typical phototransistor based on epitaxial-grown high-quality III-V materials with similar photogating effects [for example, see the study of Takanashi *et al.* (*47*), which does not rely on trap states either], we extracted the $\Delta V_{TH}$ of both devices in Fig. 4D. One can see

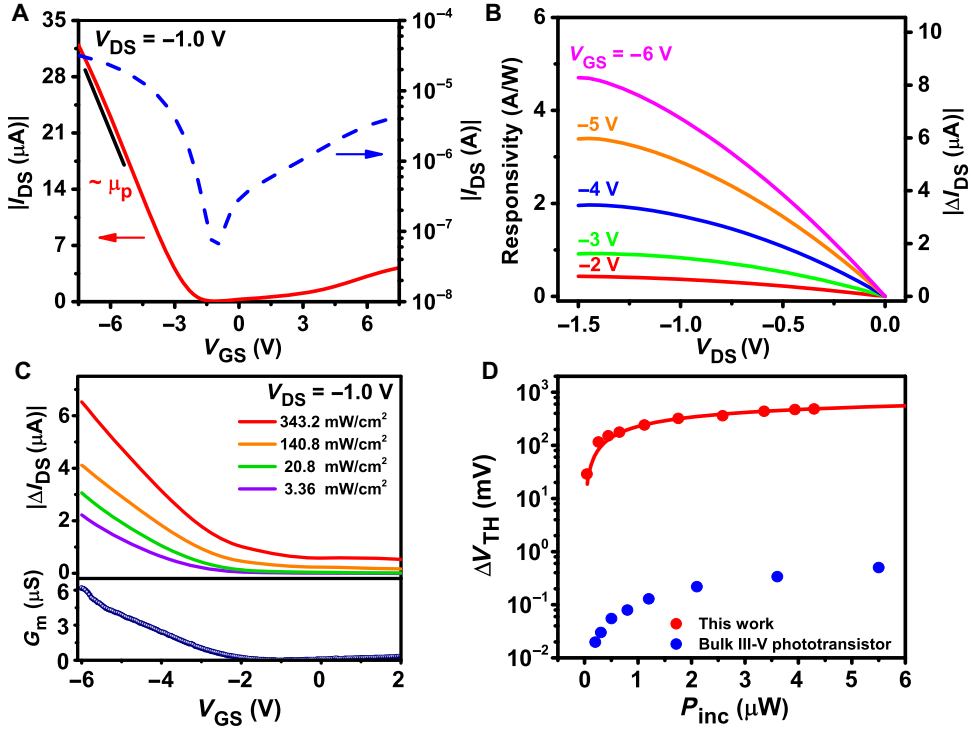


**Fig. 4. Measurements of ultrathin Ge phototransistor and its analysis.** (**A**) Transfer curves ($V_{GS}$-$I_{DS}$) of the ultrathin Ge transistor. (**B**) Photoresponsivity and $V_{DS}$-$I_{DS}$ curves of the ultrathin Ge phototransistor under the illumination power density of 140.8 mW/$cm^2$. The peak photoresponsivity is 4.7 A/W. (**C**) Top: Ultrathin Ge transistor photocurrent ($|\Delta I_{DS}|$) as a function of $V_{GS}$ under various power conditions: 3.36 (purple), 20.8 (green), 140.8 (orange), and 343.2 mW/$cm^2$ (red), respectively. Bottom: Transconductance ($|G_m|$) of ultrathin Ge transistors. (**D**) Comparison of threshold voltage change ($\Delta V_{TH}$) of the ultrathin Ge phototransistor with that of the epitaxial-based III-V phototransistor. The measured $\Delta V_{TH}$ values are obtained by subtracting the threshold voltages extracted from the $V_{GS}$-$I_{DS}$ curves under the illuminated and dark conditions (fig. S9). The solid curve is plotted using the empirical equation for $\Delta V_{TH}$.

that the $\Delta V_{TH}$ values of our single-crystalline Ge membrane–based device (red dots) are three orders of magnitude larger than those of the III-V phototransistors (blue dots). According to the empirical equation that describes the photogating-induced $\Delta V_{TH}$ [that is, $\Delta V_{TH} = (nkT/q) \times \ln[1 + (\eta q P_{inc})/(I_{dark} h\upsilon)]$ by Takanashi *et al.* (*47*)], one can relate the incident power ($P_{inc}$) with $\Delta V_{TH}$, as shown by the red curve in Fig. 4D. Here, $n$ is an empirical constant for fitting ($n = 8.94$ obtained by the least squares method), $k$ is the Boltzmann constant ($1.38 \times 10^{-23}$ J/K), $T$ is the temperature (300 K), $h$ is the Planck's constant ($6.63 \times 10^{-34}$ J·s), and $\upsilon$ is the frequency of light ($4.09 \times 10^{14}$ Hz, corresponding to 733 nm). The excellent fitting confirms that the large $\Delta V_{TH}$ is contributed by the strong absorption ($\eta$) due to the nanocavity and the effective suppression of dark current ($I_{dark}$) owing to the ultrathin Ge channel. As a result, the ultrathin Ge–based phototransistor can generate a stronger signal than a traditional III-V–based device with a similar transconductance. This enhanced photocurrent holds promise in improving the performance of thin-film photodetectors, especially because pixels of sensor arrays and imagers are increasingly miniaturized (*48*). Intriguingly, the absorption enhancement resonance can be manipulated by controlling the nanocavity structure, which will enable the development of new multispectral sensing on the same chip.

### *Spectral response and tunability: The potential for multispectral sensing on the same chip*

In addition to its benefit in electrical properties, the ultrathin thickness also provides a new optical functionality for multispectral sensing because its response exhibits strong spectral tunability. To demonstrate this tunability, here, we fabricated a series of nanocavity-manipulated photodetectors by changing the thickness of the Ge membrane on the same 220-nm $Al_2O_3$/Ag cavity. Figure 5A shows the experimentally measured light absorption spectra of these samples. As the thickness of the Ge film increases from 6 to 40 nm, the wavelength of the absorption peak changes from 715 to 862 nm, agreeing very well with numerical simulations (fig. S10). To demonstrate the spectrally tunable photoresponse, we further measured the photocurrent spectra for three photodetectors with their Ge thicknesses of 12, 17, and 26 nm, respectively, as shown in Fig. 5B (see fig. S11 for the corresponding optical microscopy images). Here, a supercontinuum laser coupled with a monochromator was used as the light source. The photoresponsivity of all devices was measured under the same bias voltage of 1 V. In Fig. 5B, the simulated light absorption spectra are also plotted by solid curves, showing excellent agreement with the measured photocurrent responsivities (dots) and demonstrating the spectral tunability. Therefore, a multispectral ultrathin Ge photodetector array is realizable by transferring different crystalline Ge membranes onto the predesigned nanocavity substrate.

## DISCUSSION

In summary, we developed a nanocavity-enhanced single-crystalline Ge nanomembrane photodetector. The fabrication processes successfully thinned down the Ge films to as thin as ~10 nm and maintained the single-crystalline material quality of the nanomembranes. The photoresponsivity could reach up to 4.7 A/W, resulting from the enhanced absorption and gate modulation. Because of the significantly reduced volume of the active material, the dark current was reduced significantly. Along with the increased photocurrent due to the enhanced optical absorption within Ge nanomembranes, the NPDR as high as ~$10^5$ $mW^{-1}$ was realized. The NPDR of our device also exhibited better stability under stronger incident power than that of 2D material devices, mainly due to the great material quality of the single-crystalline Ge nanomembranes. Furthermore, by characterizing the gate-controlled performance, the device physics of this ultrathin-film photodetector were analyzed, showing obvious photogating effect. The enhanced absorption and confinement of the carriers led to a large change of threshold voltage and thus enhanced photoconductivity. By integrating the Ge membranes (10 to 30 nm) with predesigned nanocavities, we demonstrated

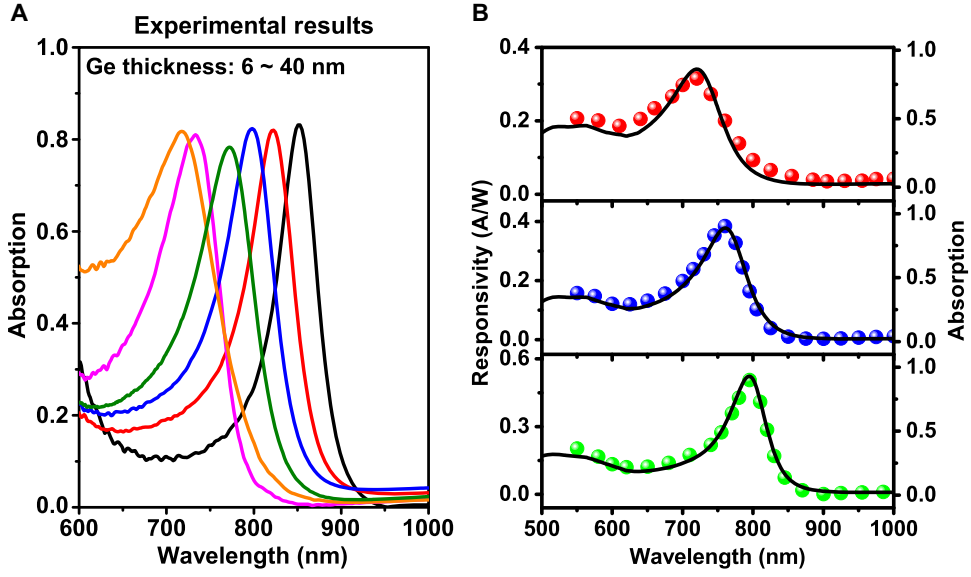


**Fig. 5. Absorption measurements of ultrathin Ge sample with varying thickness (from 6 to 40 nm) on the same chip and the spectral photocurrent response.** (**A**) Absorption spectra measured by Fourier transform infrared spectroscopy of the ultrathin Ge sample. The peak wavelength becomes larger as the Ge nanomembrane thickness changes from 6 to 40 nm. (**B**) Left axis: Photoresponsivity (A/W) results of three different samples on the same 220-nm-thick $Al_2O_3$/Ag substrate. The thicknesses of Ge films are (from top to bottom) 12, 17, and 26 nm, respectively. Right axis: Simulated absorption spectra of these three samples, with the same structure parameters mentioned above. The simulation is based on full-wave Maxwell's equations.

spectrally tunable thin-film phototransistors. Because of the complementary metal-oxide semiconductor–compatible processes, the proposed single-crystalline Ge membrane ultrathin-film transistors can be fabricated over a large scale (for example, wafer scale), which is superior to current 2D material–based optoelectronic devices and can be a competitive building block for next-generation functional electronic/optoelectronic circuits.

## MATERIALS AND METHODS

We used the smart-cut process (*49*) to fabricate the GeOI. The process started with a p-type (gallium-doped) 4-inch bulk Ge wafer. We ion-implanted a uniform $H^+$ layer in the Ge wafer with a dose of $1 \times 10^{17}$ $cm^{-2}$ and an energy of $1.602 \times 10^{-14}$ $kg{\cdot}m^2{\cdot}S^{-2}$ (fig. S1A). A $H^+$ peak position was carefully designed at 700 nm from the Ge surface to acquire a 400-nm-thick Ge layer after the exfoliating process. A 1-μm-thick $SiO_2$ layer on the Si wafer was obtained by thermal oxidation as the buried oxide layer. Then, the Ge wafer was flipped over. The $O_2$ plasma was used to clean both surfaces for bonding (shown in fig. S1B). The wafer bonding process was performed using the EVG Wafer Bonding System (EV 801) under the vacuum of $7 \times 10^{-5}$ mbar (fig. S1C). After that, a two-step, low-temperature annealing at 200° and 250°C was carried out in a nitrogen-filled oven to achieve the exfoliation of the Ge wafer (fig. S1D). The Ge membrane was very rough after the exfoliation, and a chemical-mechanical polishing process was required to polish the Ge membrane surface and thin down the Ge layer to the desired thickness (100 nm).

## SUPPLEMENTARY MATERIALS

Supplementary material for this article is available at http://advances.sciencemag.org/cgi/content/full/3/7/e1602783/DC1

Supplementary Materials

note S1. Fabrication and characterization of the laboratory-made GeOI wafer.

fig. S1. Fabrication process flow of 4-inch GeOI and its finished sample.

fig. S2. Characterization of laboratory-made GeOI.

fig. S3. The GeOI sample used for the van der Pauw measurement.

fig. S4. Thickness measurement of the corresponding ultrathin Ge membranes in Fig. 1B by AFM (XE-70 Park System).

fig. S5. Demonstration of the ultrathin Ge nanomembranes from laboratory-made GeOI to foreign substrate.

fig. S6. Titled scanning electron microscopy images of the ultrathin Ge membranes transferred onto foreign substrate.

fig. S7. Dark current measurements of different thicknesses of the Ge membrane sample.

fig. S8. The dark current and the photoresponse of the ultrathin GeOI sample.

fig. S9. $V_{GS}$-$I_{DS}$ curve under the dark and different illumination conditions.

fig. S10. Simulated absorption spectra of ultrathin Ge nanomembranes on a 220-nm-thick $Al_2O_3$/Ag nanocavity substrate.

fig. S11. Optical microscopy images of the samples for multispectral response measurement.

table S1. Electronic properties of p-type GeOI sample.

## REFERENCES AND NOTES


1. S. Xu, Z. Yan, K.-I. Jang, W. Huang, H. Fu, J. Kim, Z. Wei, M. Flavin, J. McCracken, R. Wang, A. Badea, Y. Liu, D. Xiao, G. Zhou, J. Lee, H. U. Chung, H. Cheng, W. Ren, A. Banks, X. Li, U. Paik, R. G. Nuzzo, Y. Huang, Y. Zhang, J. A. Rogers, Assembly of micro/nanomaterials into complex, three-dimensional architectures by compressive buckling. *Science* **347**, 154–159 (2015).
2. H. Ko, K. Takei, R. Kapadia, S. Chuang, H. Fang, P. W. Leu, K. Ganapathi, E. Plis, H. S. Kim, S.-Y. Chen, M. Madsen, A. C. Ford, Y.-L. Chueh, S. Krishna, S. Salahuddin, A. Javey, Ultrathin compound semiconductor on insulator layers for high-performance nanoscale transistors. *Nature* **468**, 286–289 (2010).
3. X. Liu, T. Galfsky, Z. Sun, F. Xia, E.-c. Lin, Y.-H. Lee, S. Kéna-Cohen, V. M. Menon, Strong light–matter coupling in two-dimensional atomic crystals. *Nat. Photonics* **9**, 30–34 (2014).
4. H. Yuan, X. Liu, F. Afshinmanesh, W. Li, G. Xu, J. Sun, B. Lian, A. G. Curto, G. Ye, Y. Hikita, Z. Shen, S.-C. Zhang, X. Chen, M. Brongersma, H. Y. Hwang, Y. Cui, Polarization-sensitive broadband photodetector using a black phosphorus vertical p–n junction. *Nat. Nanotechnol.* **10**, 707–713 (2015).
5. N. Youngblood, C. Chen, S. J. Koester, M. Li, Waveguide-integrated black phosphorus photodetector with high responsivity and low dark current. *Nat. Photonics* **9**, 247–252 (2015).
6. M. A. Kats, R. Blanchard, P. Genevet, F. Capasso, Nanometre optical coatings based on strong interference effects in highly absorbing media. *Nat. Mater.* **12**, 20–24 (2013).
7. K.-T. Lee, S. Seo, J. Y. Lee, L. J. Guo, Strong resonance effect in a lossy medium-based optical cavity for angle robust spectrum filters. *Adv. Mater.* **26**, 6324–6328 (2014).
8. K.-T. Lee, S. Seo, J. Y. Lee, L. J. Guo, Ultrathin metal-semiconductor-metal resonator for angle invariant visible band transmission filters. *Appl. Phys. Lett.* **104**, 231112 (2014).
9. V. Steenhoff, M. Theuring, M. Vehse, K. von Maydell, C. Agert, Ultrathin resonant-cavity-enhanced solar cells with amorphous germanium absorbers. *Adv. Opt. Mater.* **3**, 182–186 (2015).
10. D. O. Sigle, L. Zhang, S. Ithurria, B. Dubertret, J. J. Baumberg, Ultrathin CdSe in plasmonic nanogaps for enhanced photocatalytic water splitting. *J. Phys. Chem. Lett.* **6**, 1099–1103 (2015).
11. Y. Xin, L. Wu, L. Ge, C. Han, Y. Li, S. Fang, Gold–palladium bimetallic nanoalloy decorated ultrathin 2D $TiO_2$ nanosheets as efficient photocatalysts with high hydrogen evolution activity. *J. Mater. Chem. A* **3**, 8659–8666 (2015).
12. S. J. Kim, J. Park, M. Esfandyarpour, E. F. Pecora, P. G. Kik, M. L. Brongersma, Superabsorbing, artificial metal films constructed from semiconductor nanoantennas. *Nano Lett.* **16**, 3801–3808 (2016).
13. H. Song, L. Guo, Z. Liu, K. Liu, X. Zeng, D. Ji, N. Zhang, H. Hu, S. Jiang, Q. Gan, Nanocavity enhancement for ultra-thin film optical absorber. *Adv. Mater.* **26**, 2737–2743 (2014).
14. M. A. Kats, F. Capasso, Optical absorbers based on strong interference in ultra-thin films. *Laser Photonics Rev.* **10**, 699 (2016).
15. R. W. Going, J. Loo, T. J. K. Liu, M. C. Wu, Germanium gate photoMOSFET integrated to silicon photonics. *IEEE J. Sel. Top. Quantum Electron.* **20**, 1–7 (2014).
16. S. Assefa, F. Xia, Y. A. Vlasov, Reinventing germanium avalanche photodetector for nanophotonic on-chip optical interconnects. *Nature* **464**, 80–84 (2010).
17. D. Liang, J. E. Bowers, Recent progress in lasers on silicon. *Nat. Photonics* **4**, 511–517 (2010).
18. J. H. Nam, T. Fuse, Y. Nishi, K. C. Saraswat, Germanium on insulator (GOI) structure using hetero-epitaxial lateral overgrowth on silicon. *ECS Trans.* **45**, 203–208 (2012).
19. D. Kazazis, P. Jannaty, A. Zaslavsky, C. Royer, C. Tabone, L. Clavelier, S. Cristoloveanu, Tunneling field-effect transistor with epitaxial junction in thin germanium-on-insulator. *Appl. Phys. Lett.* **94**, 263508 (2009).
20. J. A. Rogers, M. G. Lagally, R. G. Nuzzo, Synthesis, assembly and applications of semiconductor nanomembranes. *Nature* **477**, 45–53 (2011).
21. M. A. Meitl, Z.-T. Zhu, V. Kumar, K. J. Lee, X. Feng, Y. Y. Huang, I. Adesida, R. G. Nuzzo, J. A. Rogers, Transfer printing by kinetic control of adhesion to an elastomeric stamp. *Nat. Mater.* **5**, 33–38 (2006).
22. C. Janisch, H. Song, C. Zhou, Z. Lin, A. L. Elías, D. Ji, M. Terrones, Q. Gan, Z. Liu, $MoS_2$ monolayers on nanocavities: Enhancement in light–matter interaction. *2D Mater.* **3**, 025017 (2016).
23. H. Song, S. Jiang, D. Ji, X. Zeng, N. Zhang, K. Liu, C. Wang, Y. Xu, Q. Gan, Nanocavity absorption enhancement for two-dimensional material monolayer systems. *Opt. Express* **23**, 7120–7130 (2015).
24. M. K. Hudait, M. Clavel, P. Goley, N. Jain, Y. Zhu, Heterogeneous integration of epitaxial Ge on Si using AlAs/GaAs buffer architecture: Suitability for low-power fin field-effect transistors. *Sci. Rep.* **4**, 6964 (2014).
25. V. Sorianello, L. Colace, N. Armani, F. Rossi, C. Ferrari, L. Lazzarini, G. Assanto, Low-temperature germanium thin films on silicon. *Opt. Matter Express* **1**, 856–865 (2011).
26. G. Masini, L. Colace, F. Galluzzi, G. Assanto, Advances in the field of poly-Ge on Si near infrared photodetectors. *Mater. Sci. Eng. B* **69**, 257–260 (2000).
27. D. Nam, D. Sukhdeo, A. Roy, K. Balram, S.-L. Cheng, K. C.-Y. Huang, Z. Yuan, M. Brongersma, Y. Nishi, D. Miller, K. Saraswat, Strained germanium thin film membrane on silicon substrate for optoelectronics. *Opt. Express* **19**, 25866–25872 (2011).
28. D. Bermejo, M. Cardona, Raman-scattering in pure and hydrogenated amorphous germanium and silicon. *J. Non Cryst. Solids* **32**, 405–419 (1979).
29. J. Wang, S. Lee, Ge-photodetectors for Si-based optoelectronic integration. *Sensors* **11**, 696–718 (2011).
30. n,k database; www.ioffe.ru/SVA/NSM/nk/index.html.
31. C. O. Chui, A. K. Okyay, K. C. Saraswat, Effective dark current suppression with asymmetric MSM photodetectors in Group IV semiconductors. *IEEE Photonics Technol. Lett.* **15**, 1585–1587 (2003).
32. L. Chen, P. Dong, M. Lipson, High performance germanium photodetectors integrated on submicron silicon waveguides by low temperature wafer bonding. *Opt. Express* **16**, 11513–11518 (2008).
33. O. Lopez-Sanchez, D. Lembke, M. Kayci, A. Radenovic, A. Kis, Ultrasensitive photodetectors based on monolayer $MoS_2$. *Nat. Nanotechnol.* **8**, 497–501 (2013).

34. P. Zhang, E. Tevaarwerk, B.-N. Park, D. E. Savage, G. K. Celler, I. Knezevic, P. G. Evans, M. A. Eriksson, M. G. Lagally, Electronic transport in nanometre-scale silicon-on-insulator membranes. *Nature* **439**, 703–706 (2006).
35. K. S. Shamala, L. C. S. Murthy, K. N. Rao, Studies on optical and dielectric properties of $Al_2O_3$ thin films prepared by electron beam evaporation and spray pyrolysis method. *Mater. Sci. Eng. B* **106**, 269–274 (2004).
36. H. Schmidt, S. Wang, L. Chu, M. Toh, R. Kumar, W. Zhao, A. H. C. Neto, J. Martin, S. Adam, B. Özyilmaz, G. Eda, Transport properties of monolayer $MoS_2$ grown by chemical vapor deposition. *Nano Lett.* **14**, 1909–1913 (2014).
37. N. R. Pradhan, D. Rhodes, S. Feng, Y. Xin, S. Memaran, B.-H. Moon, H. Terrones, M. Terrones, L. Balicas, Field-effect transistors based on few-layered α-$MoTe_2$. *ACS Nano* **8**, 5911–5920 (2014).
38. J. Kumar, M. A. Kuroda, M. Z. Bellus, S.-J. Han, H.-Y. Chiu, Full-range electrical characteristics of $WS_2$ transistors. *Appl. Phys. Lett.* **106**, 123508 (2015).
39. R. Yang, Z. Wang, P. X.-L. Feng, Electrical breakdown of multilayer $MoS_2$ field-effect transistors with thickness-dependent mobility. *Nanoscale* **6**, 12383–12390 (2014).
40. H. Zhou, C. Wang, J. C. Shaw, R. Cheng, Y. Chen, X. Huang, Y. Liu, N. O. Weiss, Z. Lin, Y. Huang, X. Duan, Large area growth and electrical properties of p-type $WSe_2$ atomic layers. *Nano Lett.* **15**, 709–713 (2015).
41. F. Xia, H. Wang, Y. Jia, Rediscovering black phosphorus as an anisotropic layered material for optoelectronics and electronics. *Nat. Commun.* **5**, 4458 (2014).
42. C. Soci, A. Zhang, B. Xiang, S. A. Dayeh, D. P. R. Aplin, J. Park, X. Y. Bao, Y. H. Lo, D. Wang, ZnO nanowire UV photodetectors with high internal gain. *Nano Lett.* **7**, 1003–1009 (2007).
43. G. Konstantatos, M. Badioli, L. Gaudreau, J. Osmond, M. Bernechea, F. P. Garcia de Arquer, F. Gatti, F. H. Koppens, Hybrid graphene-quantum dot phototransistors with ultrahigh gain. *Nat. Nanotechnol.* **7**, 363–368 (2012).
44. Q. Guo, A. Pospischil, M. Bhuiyan, H. Jiang, H. Tian, D. Farmer, B. Deng, C. Li, S.-J. Han, H. Wang, Q. Xia, T.-P. Ma, T. Mueller, F. Xia, Black phosphorus mid-infrared photodetectors with high gain. *Nano Lett.* **16**, 4648–4655 (2016).
45. J. O. Island, S. I. Blanter, M. Buscema, H. S. J. van der Zant, A. Castellanos-Gomez, Gate controlled photocurrent generation mechanisms in high-gain $In_2Se_3$ phototransistors. *Nano Lett.* **15**, 7853–7858 (2015).
46. M. M. Furchi, D. K. Polyushkin, A. Pospischil, T. Mueller, Mechanisms of photoconductivity in atomically thin $MoS_2$. *Nano Lett.* **14**, 6165–6170 (2014).
47. Y. Takanashi, K. Takahata, Y. Muramoto, Characteristics of InAlAs/InGaAs high-electron-mobility transistors under illumination with modulated light. *IEEE Trans. Electron Dev.* **46**, 2271–2277 (1999).
48. G. Konstantatos, E. H. Sargent, Nanostructured materials for photon detection. *Nat. Nanotechnol.* **5**, 391–400 (2010).
49. M. Bruel, Process for the production of thin semiconductor material films, U.S. Patent 5,374,564 A (1994).



**Acknowledgments**

**Funding:** This research was partially supported by the NSF (grant nos. ECCS1507312 and CMMI1562057). Z.M. and Z.Y. were supported by the NSF (grant nos. ECCS1405201 and ECCS1641006). Z.X., M.K., T.-H.C., D.L, K.X., H.M., and Z.M. were supported by Air Force Office of Scientific Research under a Presidential Early Career Award for Scientists and Engineers grant no. FA9550-09-1-0482 and partly by U.S. Department of Energy National Nuclear Security Administration program under grant no. DE-NA0002915. **Author contributions:** Z.Y., Z.M., and Q.G. conceived the idea. Z.X., H.S., Z.Y., and Q.G. initiated this study and designed the research program. All authors performed the experiments and data analysis. H.S. performed the simulation. Z.X., H.S., X.W., F.X., Z.Y., Z.M., and Q.G. wrote the manuscript. All authors reviewed the manuscript. **Competing interests:** Z.X., H.S., M.Z., Z.Y., Z.M., and Q.G. are authors on a patent application related to this work (15/612,187, filed 2 June 2017). All other authors declare that they have no competing interests. **Data and materials availability:** All data needed to evaluate the conclusions in the paper are present in the paper and/or the Supplementary Materials. Additional data are available from authors upon request.

Submitted 9 November 2016
Accepted 26 May 2017
Published 7 July 2017
10.1126/sciadv.1602783

**Citation:** Z. Xia, H. Song, M. Kim, M. Zhou, T.-H. Chang, D. Liu, X. Yin, K. Xiong, H. Mi, X. Wang, F. Xia, Z. Yu, Z. (J). Ma, Q. Gan, Single-crystalline germanium nanomembrane photodetectors on foreign nanocavities. *Sci. Adv.* **3**, e1602783 (2017).

Science Advances

# Single-crystalline germanium nanomembrane photodetectors on foreign nanocavities

Zhenyang Xia, Haomin Song, Munho Kim, Ming Zhou, Tzu-Hsuan Chang, Dong Liu, Xin Yin, Kanglin Xiong, Hongyi Mi, Xudong Wang, Fengnian Xia, Zongfu Yu, Zhenqiang (Jack) Ma and Qiaoqiang Gan

*Sci Adv* **3** (7), e1602783.
DOI: 10.1126/sciadv.1602783